EXECUTIVE SUMMARY

MAGNETIC FIELD PERTURBATIONS BY THERMO-ELECTRIC EFFECTS

CONTRACT NO. 4000121851/17/NL/LVH/MD

Date: *06-02-2019*
Pages: *19*
Status: *Final*
Project: Magnetic Field Perturbations by Thermo-Electric Effects
Reference: *Executive* Summary
Version: V 1.0

Partners:

CMT, BCM

EXECUTIVE SUMMARY

MAGNETIC FIELD PERTURBATIONS BY THERMO-ELECTRIC EFFECTS

Approval:				
Revision	**Name**	**Function**	**Signature**	**Date**
3	Paulo Antunes	TAM		
3	Senentxu Lanceros Mendez	Scientific Director		

Authors and Contributors:			
Name	**Contact**	**Description**	**Date**
Paulo Antunes	pjantunes@crtical-materials.com	Technical Area Manager	06-02-2019
Nelson Ferreira	njferreira@crtical-materials.com	Technical Area Manager	06-02-2019
Senentxu Lanceros Mendez	Senentxu.lanceros@bcmaterials.net	Research Professor	06-02-2019
Liliana Fernandes	liliana.fernandes@bcmaterials.net	Research Student	06-02-2019

Access List:
Internal Access
Project staff
External Access
ESA staff

Revision History:				
Revision	**Version**	**Date**	**Description**	**Author**
1	1	08-11-2019	First revision	Paulo Antunes
2	1	13-02-2019	Insertion of new information and review	Liliana Fernandes / Senentxu Lanceros-Mendez
3	1	13-02-2019	Global revision	Paulo Antunes

TABLE OF CONTENTS

1. Introduction

This report, and in the context of the ***Magnetic Field Perturbations by Thermo-Electric Effects*** ESA's project (from now on referred as ***THEMA*** project), summarize the technical activities and main results obtained during the timeline of the project.

1.1 Objective

The main objective behind this document is to highlight the main findings under the **THEMA** project.

1.2 Scope

Final report on the activities of THEMA project.

1.3 Audience

The audience of this report are the project members.

1.4 Definitions and acronyms

Acronyms	Description
CMT	Critical Materials, S.A.
BCM	Basque Centre for Materials Applications and Nanostructures
FE	Finite Element
WP	Work-Package
FEA	Finite Element Analysis
ASM	Absolute Scalar Magnetometer
VFM	Vector Fluxgate Magnetometer
FEM	Finite Element Method
CFRP	Carbon-Fibre Reinforced Polymer.

1.5 Document structure

The report is divided in six sections, including the Introduction section. The second section briefly contextualize thermoelectric and thermomagnetic effects and its impact on space applications. The section entitled "**Assessment to thermoelectric/thermomagnetic behaviour**" summarize the numerical and experimental findings towards the experimental characterization and the numerical modelling of thermoelectric/thermomagnetic effects. Mitigation actions of thermomagnetic perturbation are discussed in section number four while Conclusions and **Recommendations** and **Future Work** are outlined in sections five and six, respectively.

1.6 List of figures

1.7 List of tables

1.8 References

[1] F. Rohrman, "The Theory of the Properties of Metals and Alloys," *Journal of Chemical Education,* vol. 14, no. 2, p. 99, 1937.

[2] A. Varlamov and V. Alexey, "rediction of thermomagnetic and thermoelectric properties for novel materials and systems," *EPL (Europhysics Letters),* vol. 103, no. 4, p. 47005, 2013.

[3] T. Seebeck, "Ueber die magnetische Polarisation der Metalle und Erze durch Temperaturdifferenz," *Annalen der Physik,* vol. 82, no. 3, pp. 253-286, 1826.

[4] Y. Apertet, H. Ouerdane, C. Goupil and P. Lecoeur, "A note on the electrochemical nature of the thermoelectric power," *The European Physical Journal Plus,* vol. 131, no. 4, p. 76, 2016.

[5] J.-F. Li, W.-S. Liu, L.-D. Zhao and M. Zhou, "High-performance nanostructured thermoelectric materials," *NPG Asia Materials,* vol. 2, pp. 152-158, 2010.

[6] Z. X and L.-D. Zhao, "Thermoelectric materials: Energy conversion between heat and electricity," *Journal of Materiomics,* vol. 1, no. 2, pp. 92-105, 2015.

[7] H. Goldsmid, Introduction to Thermoeletricity, vol. Series in Materials Science 121, Springer, 2016.

[8] S. Santapuri, "Thermodynamic restrictions on linear reversible and irreversible thermo-electro-magneto-mechanical processes," *Heliyon,* vol. 2, pp. 1-26, 2016.

[9] T. Jager, J.-M. Léger and F. Bertrand, "SWARM Absolute Scalar Magnetometer accuracy: analyses and measurement results," in *Proceedings of the IEEE Sensors Conference*, 2010.

[10] E. Friis-Christensen, H. Luhr and G. Hulot, "Swarm: A constellation to study the Earth's magnetic field," *Earth Planets Space,* vol. 58, pp. 351-358, 2006.

[11] T. Jager, J. M. Léger, I. Fratter, P. Lier and P. Pacholczyk, "MAGNETIC CLEANLINESS AND THERMOMAGNETIC EFFECT: CASE STUDY OF THE ABSOLUTE SCALAR MAGNETOMETER AND ITS ENVIRONMENT ON SWARM SATTELITES," in *2016 ESA Workshop on Aerospace EMC*, Valencia, Spain, 2016.

[12] G. Hulot, P. Vigneron, J.-M. Léger, I. Fratter, N. Olsen, T. Jager, F. Bertrand, L. Brocco, O. Sirol1, X. Lalanne1, A. Boness and V. Cattin, "Swarm's absolutemagnetometer experimental vectormode, an innovative capability for space magnetometry," *Geophysical Research Letters,* pp. 1352-1359, 2015.

[13] L. Tøffner-Clausen, V. Lesur, N. Olsen and C. C. Finlay, "In-flight scalar calibration and characterisation of the Swarm magnetometry package," *Earth, Planets and Space,* p. 68:129, 2016.

[14] M. Armano, "The LISA Pathfinder Mission," *J. Phys. Conf. Ser,* vol. 610, pp. 1-18, 2015.

[15] ESA-European Space Agency, “Lisa Pathfinder,” ESA-European Space Agency, 21 Ovtober 2010. [Online]. Available: http://sci.esa.int/lisa-pathfinder/47856-picometre-precision-demonstrated-by-lisa-pathfinder-tests/. [Accessed 02 November 2017].

[16] COMSOL, "COMSOL Multiphysics," [Online]. Available: https://www.comsol.com/. [Accessed 08 06 2018].

[17] Dassault Systèmes, “Abaqus Unified FEA,” Dassault Systèmes, [Online]. Available: https://www.3ds.com/products-services/simulia/products/abaqus/. [Accessed 08 06 2018].

2. Thermoelectric and thermomagnetic effects

2.1.1 Thermoelectric effect

The thermoelectric (TE) and thermomagnetic (TM) theory phenomena in metals has been built in 1930s-1950s and it is based on the kinetic approach [1], where transport equations are formulated and solved for different systems in order to obtain the transport coefficients characterizing the TE and TM effects [2].

Thermoelectric phenomena were discovered first by Thomas J. Seebeck, who discovered that a compass needle would be deflected by a closed loop formed by two different metals joined in two places, with a temperature difference between the joints [3]. This effect illustrates the coupling of two thermodynamic potentials: the electrochemical potential and the temperature [4].

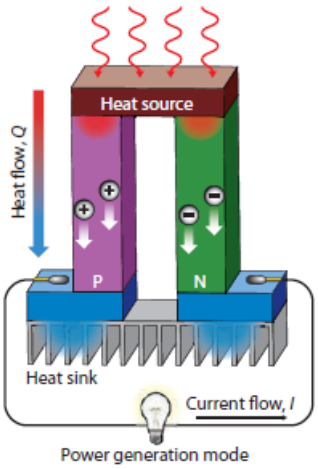

Figure 1 - Illustration of how a thermoelectric material can convert heat directly to electricity (Seebeck effect). Adapted from [5].

Thermoelectric devices have found many applications that include temperature measurement, solid-state heating or cooling and direct energy conversion from waste heat [6]. When a metallic bar is subjected to a voltage (V) or a temperature (T) difference, an electric current is generated. For small voltage and temperature gradients we may assume, in the absence of a magnetic field, a linear relation between the electric current density J and the gradients (Ohm’s law):

2.1.2 Thermomagnetic effect

While travelling in a magnetic field, electric charges are exposed to transverse forces. And by consequence, thermoelectric effects change while under the influence of the applied magnetic field and new singularities arise. The Seebeck and Peltier effects will have corresponding thermomagnetic effects, the Nernst $|N|$ and Ettinghausen $|P|$ effects [7].

In Figure 2 is graphically demonstrated the inter-relation between thermoelectric (a) and thermomagnetic effects (b).

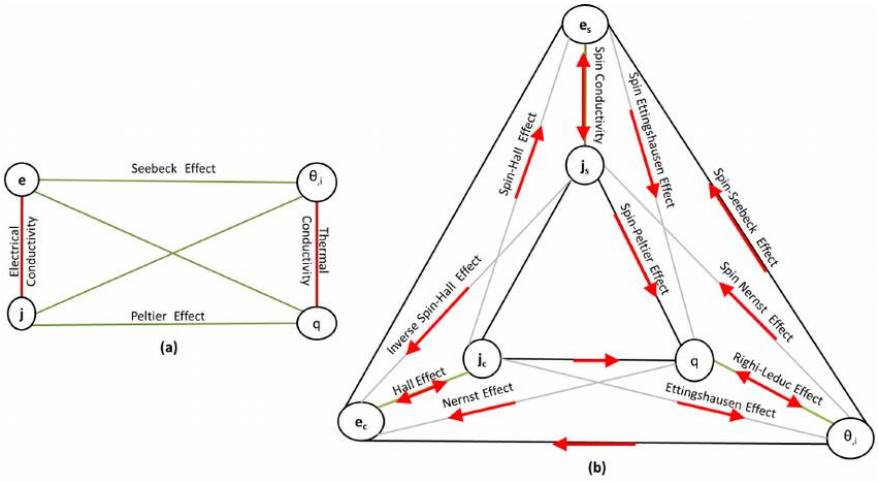

Figure 2 - Multiphysics interaction diagram (MPID) demonstrating (a) thermoelectric transport processes in the absence of external magnetic fields, and (b) galvanomagnetic, thermomagnetic, and spin-induced transport processes in the presence of external magnetic fields, in: [8].

2.2 Thermomagnetic effects in space

In the aerospace industry, the missions that require a magnetically clean spacecraft can see its performance deteriorated due to magnetic fields arising from sources that were not, à priori, considered as potential sources of magnetic field "contamination". During the extensive magnetic qualification campaign of the individual components of the ASM sensors no relevant magnetic perturbation was found as it was reported an overall precision of less than 45 pT [9]. However, during the execution of final integration tests of the SWARM satellites [10], unexpected thermomagnetic perturbation did show up in the 10nT range when the heaters, dedicated to thermal control of the Absolute Scalar Magnetometer (ASM), were activated [11]. Again according to [11], magnetic fields originated from thermoelectric currents in a Titanium (Ti) alloy bracket and brass harness lead the replacement (or removal) of those components during the on-ground satellite test campaign. The original titanium brackets, including the heaters for the thermal control of the ASM were replaced by CFRP (Carbon Fibre Reinforced Polymer). The hardware upgrade result has demonstrated efficiency as demonstrated by the reduction of thermomagnetic perturbations to the 20-30 pT $\pm$ 5 pT peak-to-peak range [11],. In mission context the SWARM satellite operation show systematic disagreements between the norm of the Vector Field Magnetometer (VFM) and the magnetic field intensity data obtained from the ASM scalar data [12], namely outside sun-eclipses. In fact, in the Absolute Scalar Magnetometer (ASM), of the three satellites of the SWARM project suffer for unforeseen magnetic disturbances, soon after launch of SWARM which could not be captured by the traditional in-flight calibration methods [13]. Also in LISA Pathfinder, a demonstration mission to validate important technologies to observe gravitational waves [14], unexpected magnetic fields created by thermal gradients were detected during the development of gold-platinum (AuPt) test mass that are used to detect gravitational waves through the continuous monitoring of the distance between them by interferometer measurements [15]. However, the origin of this magnetic perturbations is not completely understood but the microscopic inhomogeneity and grain boundaries of AuPt alloy could be contributing to the appearance of localized thermal gradients and, consequently, to differences in electric potential as result of a thermoelectric effect. The appearance of magnetic disturbances or other external disturbances can contribute to an unexpected behaviour of the test masses.

3. Assessment of thermoelectric/thermomagnetic behaviour

In this section are summarized the main experimental and numerical findings obtained during the timeline of the project

3.1 Numerical modelling of thermoelectric behaviour

3.1.1 Introduction and objectives

The use of numerical tools for the modelling of thermoelectric and thermomagnetic effects is crucial for the evaluation of the impact that those phenomena can have on environments for which the magnetic cleanness is of crucial importance. In this context, FEA tools, as a potential tool the numerical modelling of these phenomena. In fact, its intrinsic capability of 1) modelling stationary and non-stationary thermal events; 2) account different types of thermal loadings and thermal interactions; 3) consider thermal dependency on material properties (electrical and/or thermal); 4) capacity of inclusion of different materials in the same simulation domain and 5) consider geometrical complex parts; is of crucial importance for correctly account these electromagnetic effects. However, due to the non-conventionality of these phenomena, commercial finite element codes (besides COMSOL™ [16]) do not consider these effects in multiphysical simulations. In consequence it is mandatory to specialize these commercial codes to accurately simulate these phenomena. In consequence an analysis subroutine for the Abaqus™ [17] code (see Section 3.1.3) was implemented for accounting thermoelectrical effects (due to the Seebeck effect) in stationary and transient thermal analysis. Also, several post-processing tools to compute the electrical potential difference arise from the need of extracting the electrical potential difference resulting from thermal gradient considered in the simulation.

3.1.2 Thermoelectric analysis procedure

As already mentioned, Abaqus™ FE code does not account thermoelectric effect due to Seebeck effect. To overcome this situation a dedicated FORTRAN user subroutine (*UVARM) was coded to include this feature in the commercial FE code Abaqus™. The numerical procedure should allow to: 1) consider stationary and non-stationary thermal events; 2) account the temperature dependency of the Seebeck coefficient; 3) output the electric field (**E**), in equation in vectorial form.

Algorithm 1, schematizes the numerical procedure considered for the simulation of the thermoelectric phenomena. It should be noticed that the considered subroutine is called at each time increment and for each elemental integration point that compose the simulation domain.

Algorithm 1 – Thermoelectric analysis procedure

1:	**FOR** each time increment (dt):
2:	**FOR** each integration point (IP):
3:	**CALL:** Subroutine ***UVARM**
4:	**INPUT:** Thermal conductivity ($\kappa(T)$), Seebeck coefficient ($S(T)$)
5:	**CALL**: Auxiliary Subroutine ***GETVRM** and **OUTPUT** heat flux vector ($\boldsymbol{\phi}$) at integration point (IP).
6:	**CALL**: Auxiliary Subroutine ***GETVRM** and **OUTPUT** current temperature (T) at IP.
7:	**INTERPOLATE**: Seebeck coefficient (S) for the current temperature (T)
8:	**INTERPOLATE**: Thermal conductivity (κ) for the current temperature (T)
9:	**COMPUTE:** Thermal gradient ∇T through $\nabla T = \frac{\boldsymbol{\phi}(T)}{\kappa(T)}$
10:	**COMPUTE:** Electric field ($\boldsymbol{E}$) vector through: $\boldsymbol{E} = S(T)\boldsymbol{\nabla} T$
11:	**OUTPUT:** Electric field vector components (E_1, E_2, E_3)

From Algorithm 1 it is possible to that the main output is the electric field vector (originated from an electromotive force) that is computed for each element in the mesh domain. This vector field is a direct consequence of the Seebeck effect (see Equation 1) that when expressed for a steady-state condition ($\boldsymbol{J} = 0$) is given by Equation (2) and computed in the step 10 of Algorithm 1.

$$\boldsymbol{J} = \sigma(\mathbf{E} - S\boldsymbol{\nabla}\mathrm{T}) \quad (1)$$

$$\boldsymbol{E} = S\boldsymbol{\nabla}\mathrm{T} \quad (2)$$

From Equation (2) it is possible to compute the electric potential difference V (between two points a and b, through the line integral expressed in (3).

$$V_{ab} = \int_a^b \boldsymbol{E} \cdot d\boldsymbol{l} \quad (3)$$

3.1.3 Thermoelectric behaviour numerical results

3.1.3.1 Thermoelectric field

Results obtained for a cooper cylinder are shown in Figure 3 where it is possible to visualize the inhomogeneous distribution of heat flux which has a direct influence on the distribution of the electric field (Figure 3-b). The electric potential difference V_{12} (see Figure 3-c) and V_{34}, is equal to 1.1408mV and 1.040mV, respectively.

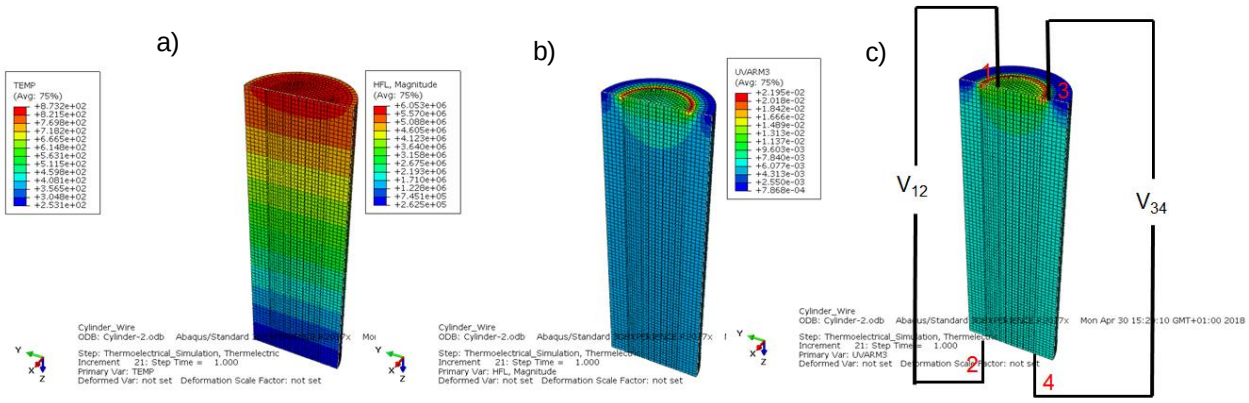

Figure 3 – Results for model 2: a) Temperature; b) Electric field (E_3) and c) points for electrical potential measurement.

Results obtained with the numerical procedure proposed were successfully validated through comparison with results obtained with COMSOL™ multiphysics commercial package, for the same geometry, loading conditions and material.

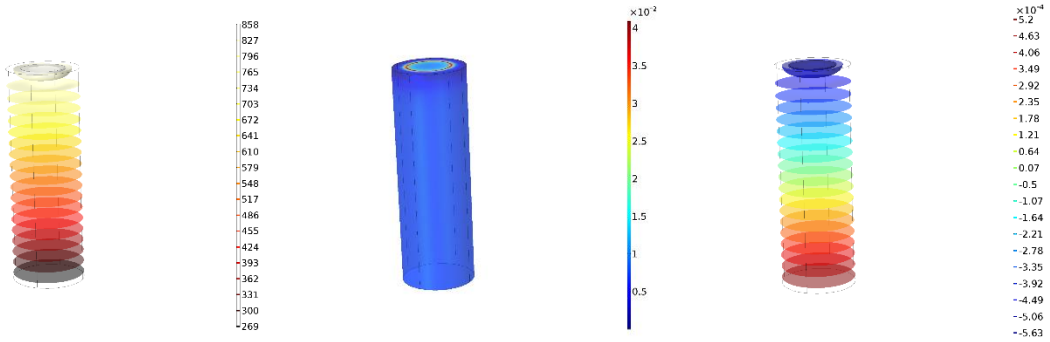

Figure 4 – Results for model 2: a) Temperature; b) Electric field (E) and c) electrical potential.

3.2 Numerical modelling of thermomagnetic behaviour

3.2.1 Introduction and objectives

In this section are detailed the numerical analysis procedure proposed for the modelling of the thermomagnetic behaviour, together with the thermomagnetic results obtained for a well-known case-study documented in the literature [11]. The proposed thermomagnetic analysis procedure proposed was implemented in Abaqus™ FEA package, making use of the intrinsic capabilities of this software package that allows the creation of dedicated analysis subroutines and results post-processing scripts.

3.2.2 The thermomagnetic analysis procedure

The coupled thermoelectric/thermomagnetic analysis procedure is divided into three different steps that should be considered sequentially:

1) *Thermoelectric analysis;*

2) *Extraction of electrical loading via post-processing script;*

3) *Thermomagnetic analysis.*

In Figure 5 is summarized the coupled thermoelectric/thermomagnetic analysis procedure proposed.

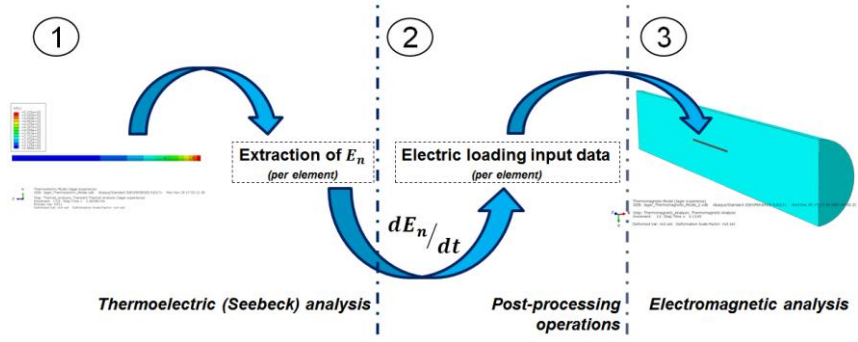

Figure 5 - Coupled thermoelectric/thermomagnetic analysis procedure, where 1, is the thermoelectric analysis block, 2 the post-processing block and 3, the thermomagnetic analysis block.

This block of post-processing operations is responsible for extracting thermoelectric results and computing the electrical current density vector per each element that will be considered in the subsequent thermomagnetic analysis procedure. In Algorithm 2 is summarized the results post-processing procedure considered for the extraction of the thermoelectrically induced electrical current density.

Algorithm 2 – Post-processing operations (electrical current density loading)

```
1:  FOR: each element in thermoelectric domain:
2:      FOR: each component (n):
3:          INCREMENT AMPLITUDE: i += 1
4:          OPEN DATA FILE: AMPLITUDE i
5:          EXTRACT: En (Electrical field per component):
6:          FOR: each time increment (dt)
7:              COMPUTE: Jn through the derivative dEn/dt
8:              WRITE TO DATA FILE: AMPLITUDE i
```

The final result of this post-processing block is a data file that fully defines the electrical loading (per element and time) in function of the thermal loadings imposed and consequent thermoelectric response obtained. The data file is composed by different electrical current density transients (three per element) that are defined per element and vector component. It should be noticed that this data file is called by the thermomagnetic analysis procedure and fully defined the thermomagnetic phenomena transiency.

3.2.3 Thermomagnetic analysis case-study

In this section are outlined the characteristics of the FE models considered for the modelling of the experimental case reported in [11]. Also, the main results obtained with the proposed thermomagnetic analysis procedure are highlighted.

3.2.3.1 The FE (thermal) model

The thermoelectric model of the rod was defined with two different convective heat transfer coefficients (top and bottom surfaces) as seen in Figure 6. The initial temperature of the rod (T_0) was set to 293.15K equal to the surrounding temperature (T_{amb}). A thermal gradient was applied to the rod considering T_{hot} equal to 523.15K and T_{cold} equal to 293.15K, being constant with time.

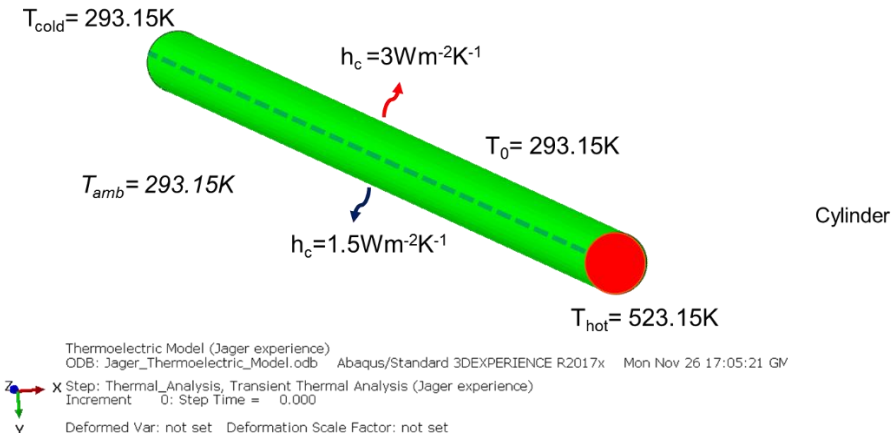

Figure 6 – Thermal boundary conditions considered for the rod.

The thermoelectric model was composed by, approximately, 50.000 (linear) elements and thermal conductivity and specific heat considered to be dependent on temperature. Seebeck

coefficient for Titanium ($3.3\mu VK^{-1}$) considered to be not-dependent on temperature and thermoelectric based vector fields computed via the dedicated analysis subroutine.

3.2.3.2 *Thermoelectrical loading scheme and thermomagnetic model*

In Figure 7 is shown the thermomagnetic model where is visible the Ti rod (conductive region) and the surrounding air (non-conductive region).

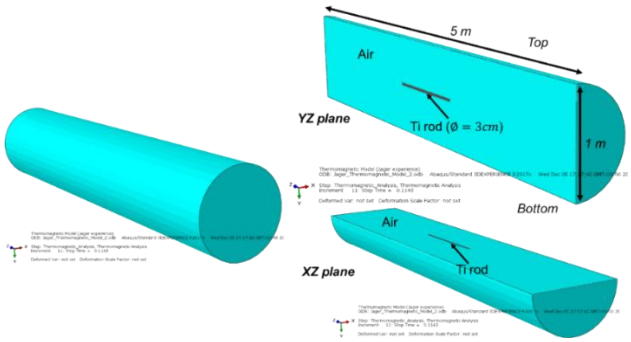

Figure 7 – Thermomagnetic model (air + rod) and two different section-cuts.

3.2.3.3 *Results*

Thermoelectric variables

From the thermoelectric analysis block, in relation to the thermal conditions considered are obtained the electrical current density values for the entire rod domain. In Figure 8 is shown the evolution, with analysis time, of the electrical current density (**J**) for two different points in the YZ plane of the rod. It is visible a non-symmetric behaviour of the electrical response for the first and second component of **J**. This behaviour is due to the differential convective heat transfer coefficient imposed to the rod's top and bottom surfaces that conditionate the heat fluxes on the rod.

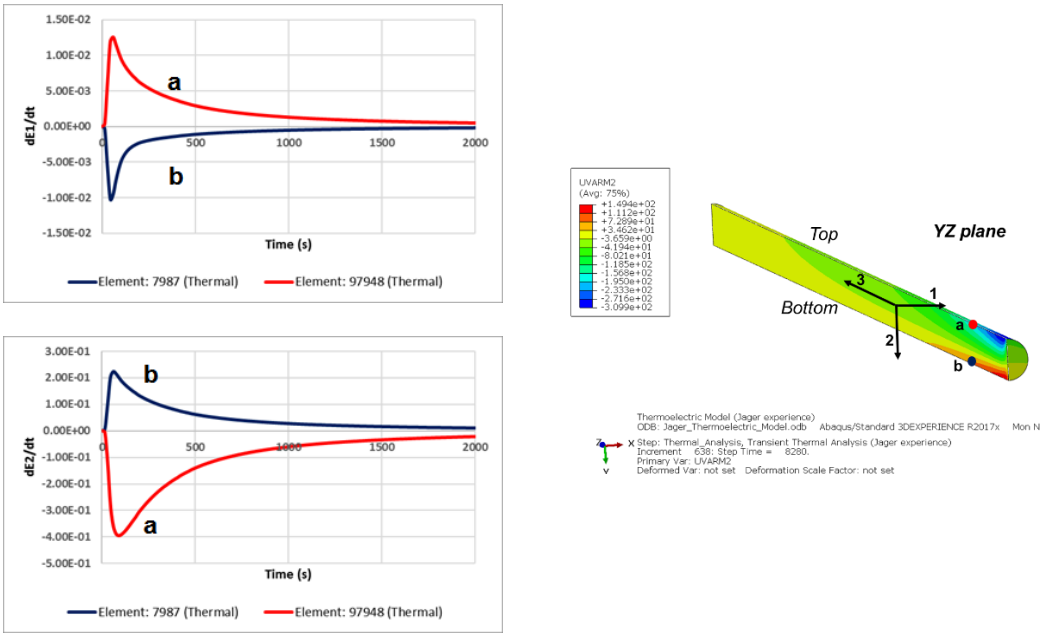

Figure 8 – Transient of electrical current density (1 and 2 components) for two different elements.

Thermomagnetic variables

The asymmetry of the magnetic flux density field (**B**) is perfectly visible on Figure 9.

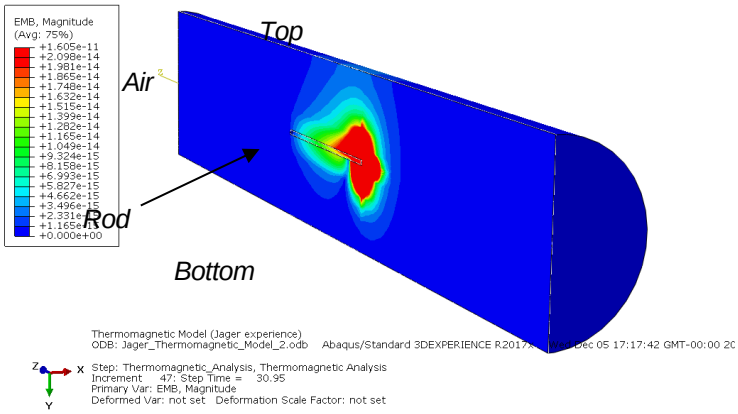

Figure 9 – Magnitude of magnetic flux density for t≈31s (YZ plane).

From the observation of Figure 9 and Figure 10 it is possible to conclude that the thermomagnetic field is dependent on the rod's angle, indicating the possibility of magnetic polarization. In fact, observing the complementary information on Figure 11 and Figure 12 is possible to conclude that the thermoelectric response originated by the rod's thermal loading conditions induces magnetic polarization on the rod's surrounding air.

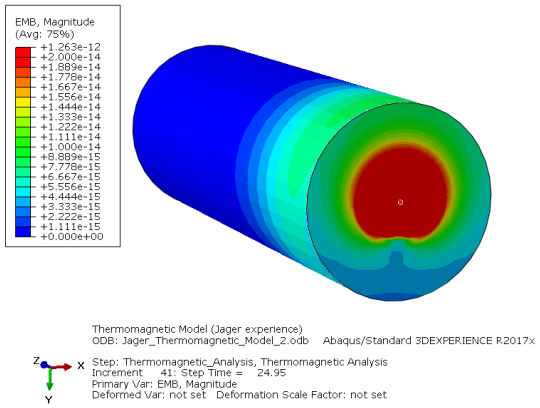

Figure 10 – Magnetic flux density field (magnitude component) for t≈25s (XY plane).

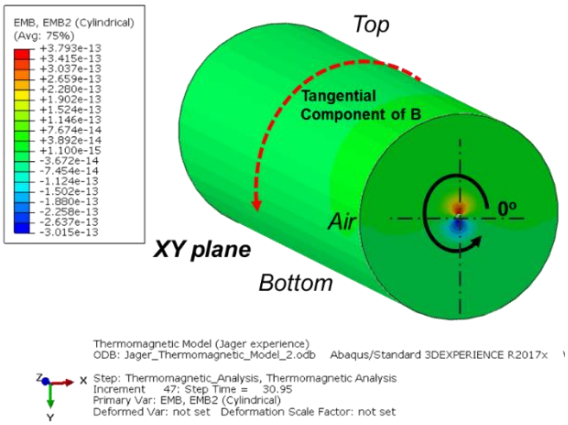

Figure 11 – Magnetic flux density field (tangential component) for t≈25s (XY plane).

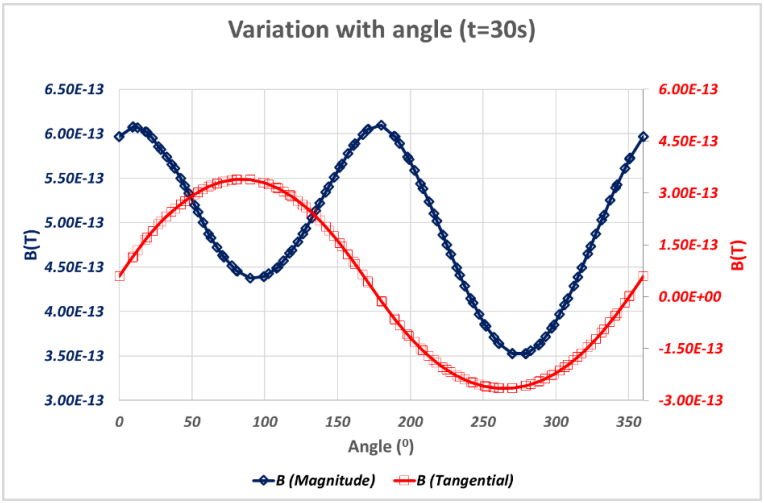

Figure 12 – Variation of the magnitude (in blue) and tangential component (in red) of magnetic flux density with rod's angle.

The 3D graph displayed in Figure 13 summarizes the dependence of the magnetic flux density field with rod's angle and analysis time. From the analysis of Figure 13 it is visible that the magnetic flux density decays with time which is in accordance with the thermoelectric loading profiles defined. Also, the minimum value of magnetic field is obtained at 270º, corresponding to the bottom region of the rod, where the heat flux rate is minimum due to the differential heat convection coefficient considered for the rod's perimeter.

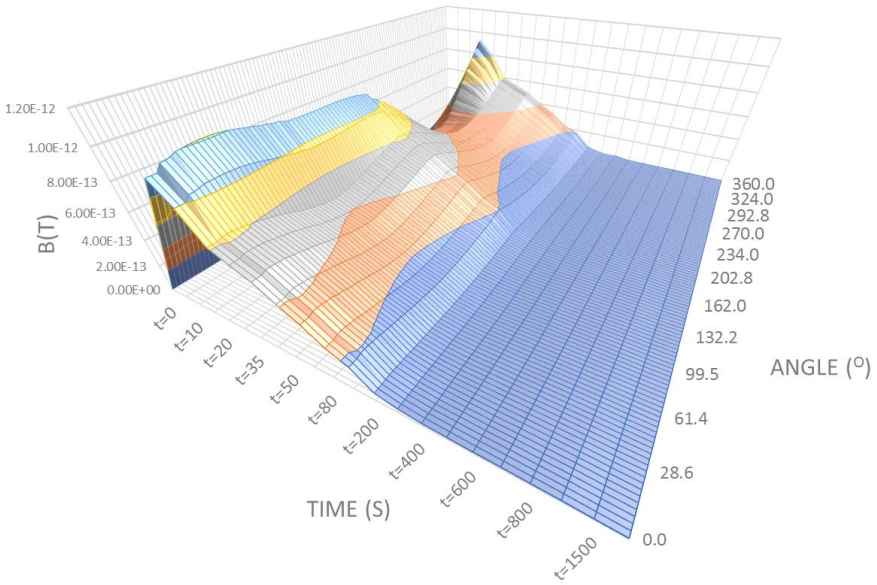

Figure 13 – Variation of the magnitude flux density (magnitude component) with rod's angle and analysis time, for a specific rod's axial position.

3.3 Experimental findings

The main goal of the experiments was to evaluate the reliability of the results obtained with the different simulations with three interrelated experimental procedures.

(i) Analysis of the produced currents from applied temperature variations. For that, a copper wire connected to Peltier cells in its extremities was subjected to different temperatures and the resulting current intensity was measured.

(ii) With an idea of the magnitude of the generated currents from experiment one, currents of the same magnitude (or higher) were applied to the same copper wire and the produced magnetic field was measured.

(iii) The wire was placed with a temperature variation under an external magnetic field in order to evaluate if there are any variations when compared with the first experiment.

3.3.1 Results

As it was mentioned in TN02 a shield assembly, from Schonstedt Instrument Company, flux gate sensor, Mag585 from Bartigton and the cylindrical sample placed in a PCB board were used (more details about the devices are in TN02). In addition, a homemade Helmholtz coil was built and a Rigol DP832 programable DC power supply and Keithley 6430 sourcemeter, to apply smaller currents in the µA range, were used as shown in Figure 14.

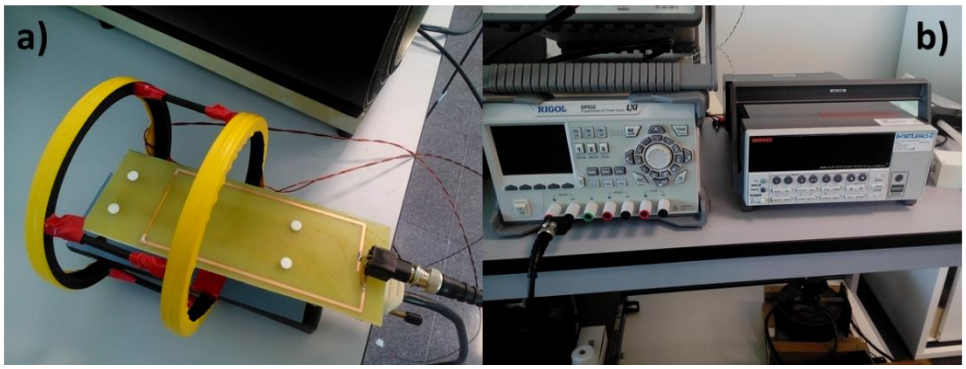

Figure 14 - a) setup of the PCB board with the copper cylindrical sample placed over the fluxgate sensor and centered in the Helmholtz coil and b) Rigol power supply (left) and Keithley sourcemeter (right).

3.3.1.1 Results

Attempts to reduce the background level in the measurements were carried out initially by placing the fluxgate sensor centered inside the Helmholtz coils, in the shield assembly and controlling the applied magnetic field with the Rigol power supply. Initially, the background had a value of 0.24 µT and the lowest baseline obtained with the coils was of ~72 nT with 1 mA steps providing defined step changes in the magnetic field with good linearity as presented in Figure 15 a). A trendline from this was traced, Figure 15 b), and magnetic field values were calculated for the predicted current values of the simulations which will be discussed later.

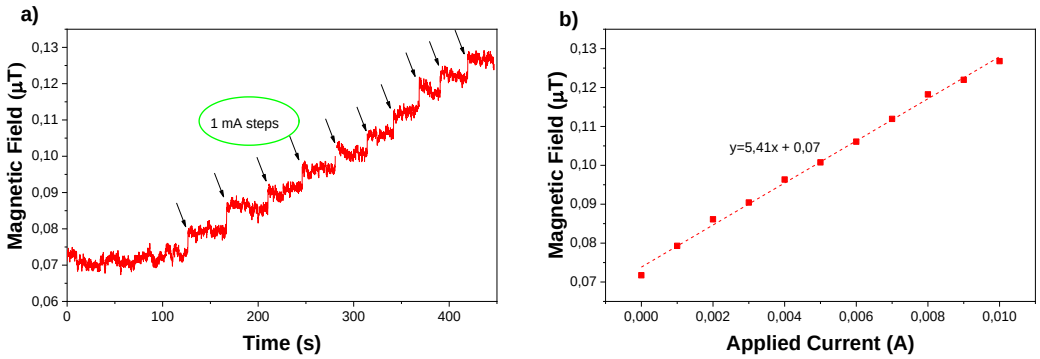

Figure 15 – a) Magnetic field increment as a function of time for 1 mA current increments and b) magnetic field correlation with the applied current.

With the introduction of a resistance in the coil, a lower background of ~7 nT was obtained with this setup. In this case, steps from 500 and 300 µA produced measurable changes in the total magnetic field as well, with the same relation as for the first attempt in reducing the

background as presented in Figure 16. In Figure 16 a) it can also be observed the reproducibility of the produced magnetic field at 1000 µA.

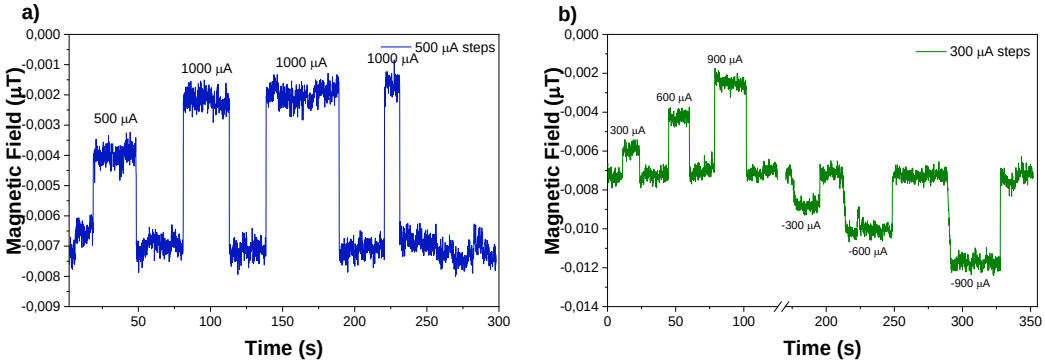

Figure 16 - Magnetic field increment as a function of time for 500 µA a) and 300 µA b) current increments.

The same linear relation as before was observed for the magnetic field with the applied current, Figure 17 with good correlation to the previous results.

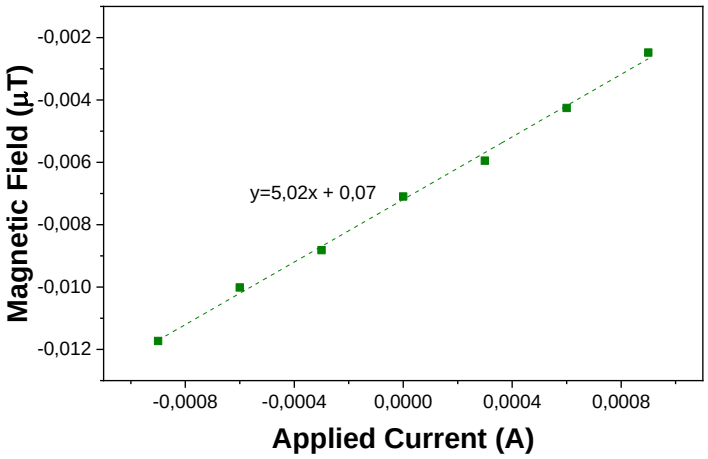

Figure 17 – Magnetic field correlation with 300 µA current steps.

With the previous results, the sensitivity needed to measure the magnetic fields generated from thermal currents was still not met. As an alternative route, a comparison was performed taking into account the simulated and experimental results, as indicated in Table 1. Only smaller temperatures were considered due to the abnormalities for higher temperatures reported in TN02 with COMSOL™ simulations.

Table 1 – Results for the simulated data compared with the data obtained experimentally.

ΔT (K)	Current (A)	Simulated Mag Field (T)	Experimental Mag Field (1 mA) (T)	Experimental Mag Field (300µA) (T)
10	2.94×10^{-8}	2.75×10^{-13}	1.50×10^{-13}	1.48×10^{-13}
20	2.94×10^{-7}	2.75×10^{-12}	1.50×10^{-12}	1.48×10^{-12}
40	5.88×10^{-7}	5.51×10^{-12}	3.18×10^{-12}	2.95×10^{-12}

80	1.18×10^{-6}	1.10×10^{-11}	6.38×10^{-12}	5.92×10^{-12}
160	1.18×10^{-5}	1.10×10^{-10}	6.38×10^{-11}	5.92×10^{-11}

A suitable match between the simulation and experimental values are observed with the background reduction. The discrepancies in the values can be attributed to various factors such as, the noise contribution of the PCB board and setup and impurities in the copper cylinder.

4. Thermomagnetic Perturbation Mitigation Techniques

In Table 2 is summarized the actions that could be followed towards the minimization of thermomagnetic perturbations. Also, the effect on the major drivers of thermomagnetic perturbations is briefly described, for each action considered.

Table 2 - Actions and effects towards the minimization of thermomagnetic perturbations.

Actions	Effect
Maximization of the thermal conductivity of selected materials, for equivalent value of Seebeck coefficient	Minimize the spatial thermal gradient and the time needed to reach a thermal steady state response.
Decrease component's mass through topological optimization.	Reducing the component's mass decreases the time to reach a thermal steady-state response, minimizing thermomagnetic perturbation through the minimization of electrical current density.
Improve the thermal insulation of metallic components more susceptible to generation thermoelectric currents through the exposition to high thermal gradients.	• Minimization of heat flux; • Minimize spatial thermal gradient; • Minimize the variation of thermal gradient with time and consequent generation of electrical current density; • Keeps the component at a steady-state thermal condition (no electrical current density generation).
Select materials with reduced Seebeck coefficients.	Minimization of electrical potential difference and electrical flux density values for a given temperature.
Reduce the number of metallic parts	Being metallic materials more susceptible to thermoelectric currents, the reduction of the number of metallic parts (and its substitution to non-metallic materials) contribute to the minimization of thermoelectrical driven currents and, consequently, thermomagnetic perturbation.
Avoid junctions of different metals	Sustainable circular currents could be generated, and a constant magnetic field is generated if the loop is closed (see Seebeck experiment)

Avoid magnetic polarized or polarizable materials	The effect of temperature on a permanent or magnetisable material changes its *B* value.
Use materials with $\mu = 1$.	The effect of the material in the presence of a magnetic field must not change the *B* magnetic field lines.

5. Conclusions

The technical activities covered during the project allowed the creation of several numerical tools that can predict the thermoelectric/thermomagnetic response to different thermal loading conditions, material properties (thermal and electrical) and geometrical configurations.

Several numerical studies were performed using both commercial and dedicated numerical analysis procedure for the assessment of the thermoelectric behaviour of simple geometries under specific thermal loading conditions.

Thermomagnetic response was exclusively obtained using the proposed numerical methodology, which allowed a detailed characterization of the thermomagnetic effect on several case-studies. It should be referenced that, on the knowledge of the authors, the modelling capabilities of the thermomagnetic analysis technique proposed in this project are not covered by any solution available on the market;

An exhaustive state-of-the-art review was performed covering the mains aspects of thermoelectric/thermomagnetic effect, and served as the theoretical basis for further developments in the context of the project

Experiments were designed to validate and thermomagnetic phenomena simulations. However, the sensitivity needed for measuring the magnetic fields generated by thermal currents was not fully obtained. On the other hand, indirect assessment of the results indicate a suitable match between the experimental results and the simulations.

The techniques proposed have great potential of use in the design of sensitive systems, namely the ones that require the maximum of magnetic cleanliness. This is the case of in-space measuring systems that require the minimum of magnetic perturbation for performing accurate measurements.

6. Recommendations and Future Work

Based on the project outcome several recommendations can be made in order to enhance the applicability of the techniques developed during the timeline of the project:

1) Define a dedicated and exhaustive plan for the qualification of the proposed thermomagnetic analysis procedure, considering several experimental case-studies and the respective numerical models for experimental/numerical correlation studies - to reflect in-orbit conditions, experimental case-studies should consider thermal radiation loading and rotation of the system in relation to a fixed radiation source;

2) Apply for an R&D project with the final goal of delivering an integrated and qualified solution for the thermomagnetic response assessment of highly sensitive systems;

3) The potential benefits of the use of the proposed numerical modelling techniques should be clearly demonstrated near potential users in order to potentiate its use during preliminary phases of system design, towards the minimization of thermomagnetic perturbation via an optimized structural design driven by the reduction of thermomagnetic perturbations.